Metrologia

PAPER

Axial force radiometer for primary standard laser power measurements using photon momentum

IOP Publishing | Bureau International des poids et mesures Metrologia

Metrologia **58** (2021) 015010 (9pp) https://doi.org/10.1088/1681-7575/abcd81

Axial force radiometer for primary standard laser power measurements using photon momentum

Paul A Williams*, Kyle A Rogers, Joshua A Hadler, Alexandra B Artusio-Glimpse and John H Lehman

National Institute of Standards and Technology, Boulder, CO, United States of America

E-mail: paul.williams@nist.gov

Received 29 July 2020, revised 29 October 2020
Accepted for publication 24 November 2020
Published 11 January 2021

Abstract

We have demonstrated operation of a new photon momentum radiometer for measuring laser power levels above 1 kW by use of radiation pressure. The 'axial' design allows the input and output laser beams to remain collinear and the force sensing can be carried out with any analytical balance having a vertical sensing direction and sufficient readability (sensitivity). The design also provides for a parasitic fast photodiode power measurement that is calibrated *in situ* by the slower radiation pressure-based power measurement. This permits a short-time-constant measurement limited primarily by the photodiode bandwidth, rather than the response time of the force balance. Uncertainty contributions yield a relative expanded uncertainty of 2.1% for (1–2) kW and 1.2% above 2 kW (for laboratory environmental conditions). We perform a direct comparison between this new power meter and the existing primary standard radiation pressure power meter. We find the two techniques agree with an average inequivalence of 0.12% for continuous wave (CW) optical powers from (1–10.8) kW. This disagreement is well-explained by the quadrature-summed uncertainties of the two techniques.

Keywords: radiation pressure, laser radiometry, power meter

(Some figures may appear in colour only in the online journal)

1. Introduction

High average-power continuous wave (CW) lasers are quickly increasing in abundance [1], capacity, and importance, for their rapid and targeted delivery of heat for applications such as cutting, welding, sintering, drying, and annealing. A portion of these applications require high-accuracy measurements of the delivered laser power. In these cases, the accuracy of 'off-the-shelf' thermal power meters (typically 3%–5%) may not be sufficient. Previous work has shown that for the highest accuracy, primary standard power meters based on photon momentum (radiation pressure) offer several advantages including faster response, smaller and more portable devices, and non-exclusive operation (allowing laser power to be fully measured during operation) [2]. We refer to this type of devices as a photon momentum radiometer (PMR). At the core of such a device is a high reflectivity mirror (sensing mirror) attached to a force sensor which measures the force of the reflected photons. We currently have two deployable implementations of PMR. The first is called the radiation pressure power meter (RPPM) [2]. This device has been successfully demonstrated for laboratory and operational settings and at power levels from 1 kW to 50 kW [3]. The design of the RPPM is especially beneficial in terms of the beam size that can be accommodated for a given power meter volume. The second implementation, which we call the axial force radiometer (AFR) [4] will be the focus of this paper.

The AFR compliments the RPPM in three areas. First, the RPPM design deflects the incoming beam by 90° which prevents it from being inserted into a previously aligned laser

* Author to whom any correspondence should be addressed.

setup. The AFR is designed for collinearly propagating input and output laser beams. Second both designs use commercial analytical balances (force balance) to measure the laser's force. The RPPM holds the sensing mirror in a vertical plane to measure a horizontally-directed laser beam. Consequently, the RPPM requires that the force balance be able to measure a horizontally directed force. This is uncommon among commercial force balances, and to enable the use of a variety of force balances, we designed AFR for a vertical force delivery—which also simplifies alignment of the laser beam. Third, the AFR allows use of a parasitic photodiode measurement of the small fraction of light leaking through a mirror to yield a significant increase in the measurement bandwidth.

Here we fully demonstrate the AFR, describe its design, detail its uncertainty analysis, and perform validating measurements with the RPPM from 1 kW to 10.8 kW. We see good agreement between the RPPM and the AFR that is well-within the uncertainties of the two instruments.

The use of photon momentum to assess optical power has been demonstrated for over a century [5, 6]. Light reflecting from a mirror experiences a change in its momentum. This results in a force F on the mirror which is directly proportional to the laser power P such that

$$P = cF/2r\cos(\theta), \tag{1}$$

where $r = R + (1-R)\alpha/2$ accounts for the fact that an absorbed photon imparts all of its momentum and a reflected photon imparts twice its momentum. R is the mirror reflectivity and α is the fraction of non-reflected light absorbed by the mirror, and θ is the angle of incidence on the mirror.

Numerous implementations of the phenomenon of equation (1) have been published with a variety of force sensing mechanisms including torsion balances [5–9], pendula [10, 11], cantilevers [12, 13], linkages [14], and microelectromechanical systems [15]. For high-average power lasers in the kilowatt regime and above, the radiation pressure forces are sufficient to permit the use of commercial analytical balances (force balances) as the sensing mechanism. This greatly simplifies the design and assembly of a PMR. This makes kilowatt-level primary-standard laser power metrology more accessible to both the laser laboratory and the laser-based manufacturing facility. The ultimate goal is for relatively low-cost primary standard power measurement capability at the point of use of high power laser functions.

2. Instrument design

The design for the AFR is seen in figure 1. The external aluminum support housing is an approximate cube with a 30 cm × 30 cm base and a height of 33 cm. Laser light enters a 70 mm diameter aperture at a center height of 27 cm and exits a symmetrically placed aperture on the opposite side. Three mirrors redirect the beam as shown in figure 1. The horizontal incoming light is directed by a turning mirror onto the sensing mirror which is connected to the force balance. Light reflected from the sensing mirror is redirected by the second turning mirror to exit the device colinearly with the incoming beam.

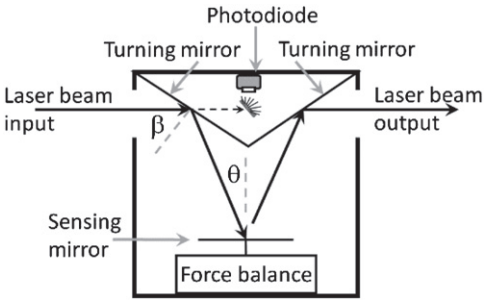

Figure 1. Layout of the axial force radiometer (AFR) geometry. Incoming laser goes through circular input aperture, hits first turning mirror at an angle of incidence β, is reflected to the sensing mirror with an incidence angle of θ, and then proceeds symmetrically to the last turning mirror and exits the second aperture colinear to the incoming beam. Laser light transmitted through the first turning mirror is incident on a scattering plate and measured with a photodiode.

This geometry facilitates the three design goals. First, the collinear input and output beams mean that the AFR can be inserted and removed from the beam path without affecting the final beam direction. This is a significant step toward a truly non-perturbing laser power meter. Second, this design permits the use of a force balance in a 'vertical force' configuration which corresponds to the operating orientation of most commercial analytical balances. This design also reduces sensitivity to operator errors in alignment. As seen in equation (1), errors in the angle θ between the laser beam and the mirror normal will cause errors in the measured power. This reduced sensitivity to device alignment will be discussed in section 3.

Third, the highly reflective turning mirrors permit a small 10–20 parts per million (ppm) fraction of the incident light to be transmitted into the triangularly shaped top compartment (figure 1). A variety of sensors (fast photodiode, beam profile camera, spectrometer, etc) can be placed there to intercept and analyze the transmitted beam simultaneous to the power measurement. For the demonstration here, we have included a photodiode to provide a fast but uncalibrated measure of the time dependent laser power. Using this configuration in tandem with the measurement from the force balance permits *in situ* calibration of the photodiode for high accuracy and high bandwidth measurement of the incident laser power.

Collinearity of the input and output laser beams requires that $\theta = 2\beta - \pi/2$. We have designed the power meter for incidence angles of $\theta = 22°$ and $\beta = 56°$. The choice of these involve a tradeoff. From equation (1) sensitivity to angular misalignment is lowest for small values of θ, but decreasing θ increases the required instrument height or diameter of the turning mirrors.

The maximum beam size is limited by a 70 mm diameter aperture chosen to accommodate typical collimated beam diameters of (1–20) kW lasers. The aperture slightly underfills the 83.9 mm vertical dimension of the 150 mm diameter

turning mirror projected at 56°. The sensing mirror is smaller (100 mm diameter), which is possible due to the smaller 22° angle of incidence.

In the following section, the various critical elements of the AFR are described and their contributions to measurement uncertainty are quantified.

2.1. Mirror design

Two performance requirements for the mirrors are that they provide high reflectivity to avoid heating from absorbed laser light and that they do not significantly distort the beam. To achieve high reflectivity, we use a Bragg mirror deposited onto a fused silica substrate using the ion beam sputtering (IBS) technique. This yields coatings with reflectance on the order of 0.999 98–0.999 99 at our operating wavelength of 1070 nm. This reflectance is measured as the fraction of incident light that is not transmitted into the mirror. That is, our 'reflectance' value includes not only specularly reflected light but also scattered light. For the purpose of these mirrors, this represents a negligible difference.

Minimizing the weight of the sensing mirror is important to avoid overloading the force balance. But this is a tradeoff—thinner mirrors weigh less but are more prone to distortion from compressive stress induced by the coating, which causes the mirror to take-on a slight convex deformation (spherical to first order). We do not require 'optical flatness' but wish to minimize distortion of the beam shape upon reflection.

The most significant problem with spherical mirror curvature is the elliptical distortion of the reflected beam. A laser beam with a circularly symmetric transverse beam profile will produce an identical circular beam when reflecting at any angle from a planar mirror but yields an elliptical beam profile if the mirror has a spherical curvature. The resulting beam shape is a function of the mirror's radius of curvature ρ, the diameter a of the incoming beam, and the angle of incidence φ on the mirror. The reflected diameter D of the beam is a function of the distance z from the mirror at which the diameter is reported

$$D_{\parallel} \approx a\left(1+\frac{2z}{\rho\,\cos\,\varphi}\right) \tag{2}$$

and

$$D_{\perp} \approx a\left(1+\frac{2z\,\cos\,\varphi}{\rho}\right), \tag{3}$$

where $D_{\parallel}$ and $D_{\perp}$ are the beam diameter in the direction parallel and perpendicular to the plane of incidence, respectively, and the approximation assumes operation in the paraxial limit $a/\rho \ll 1$. As an example, a circularly symmetric incident beam reflecting at 45° from a mirror with a 20 m radius of curvature will have an ellipticity ($D_{\parallel}/D_{\perp}$) of 1.4 when sampled 10 m from the mirror. We see that in the far field ($z/\rho \gg 1$), the ellipticity of the beam ($D_{\parallel}/D_{\perp}$) will approach $1/\cos^2(\varphi)$.

The IBS mirror deposition consists of an (8–10) μm thick multilayer Bragg coating of alternating layers of SiO_2 and Ta_2O_5 with a compressive stress on the order of ∼190 MPa. The relationship between coating stress and the resulting radius of curvature ρ of the substrate is described with the Stoney equation [16]

$$\rho = \frac{E_s {h_s}^2}{6\sigma_f h_f (1-\upsilon_s)}, \tag{4}$$

where E_s is Young's modulus of the mirror substrate, h_s is the substrate thickness, σ_f is the stress of the mirror film, h_f is the mirror film thickness, and ν_s is Poisson's ratio of the substrate. Experimentally, we find these coatings on 1 mm thick substrates yield unacceptably small radii of curvature ranging from 11 m to 18 m.

Such a curvature can be mitigated with thicker substrates, which is the preferred solution for the two turning mirrors which are 3 mm thick. But, to save weight, a 1 mm thick sensing mirror is used. We mitigate the coating strain by applying a strain-balancing coating on the back surface of the substrate. This coating is of comparable thickness and composition to the mirror coating with the goal of producing an equal and opposite strain. This implementation results in 1 mm thick high reflectivity mirrors with radii of curvature greater than 100 m.

We also found that mechanical effects of the mounting can be detrimental. We originally experimented with securing the sensing mirror in its mount using four nylon hold-down screws. But the strain induced by this edge clamping was sufficient to produce significant mirror distortion. Therefore, during a measurement, the sensing mirror is held in place by only gravity.

2.2. Photodiode implementation

Present high-accuracy and high-sensitivity (readability) commercial force balances typically take ∼5 s ('response time') to reach 99% of their final value. This creates a 'dead time' at the start of laser injection and limits the frequency response of radiation-pressure-based laser power measurement. This timescale is fast compared to primary standard thermal power meters (particularly those targeting multi-kilowatt operation) but is not fast enough to measure short <5 s injections or to monitor laser power fluctuations. To mitigate this effect, we have implemented a parasitic photodiode in the design of the AFR in order to improve two aspects of power meter performance—temporal response and measurement stability. We mitigate this with a photodiode power monitor located behind the first laser turning mirror (figure 1). The finite reflectivity of the turning mirror (0.999 98–0.999 99) means a very small fraction (10–20) ppm of the incident light will transmit through the turning mirror. By placing a photodiode behind the first turning mirror, we can sample the beam power with a response time limited primarily by that of the photodiode.

The voltage output of the photodiode cannot be directly used as an absolute measure of laser power because of the significant uncertainty in the fraction of the total laser light that is incident on the photodiode. Insufficient knowledge of mirror transmission, overfilling the photodiode aperture, polarization, and speckle effects contribute to the photodiode's overall measurement uncertainty. Instead, we calibrate the

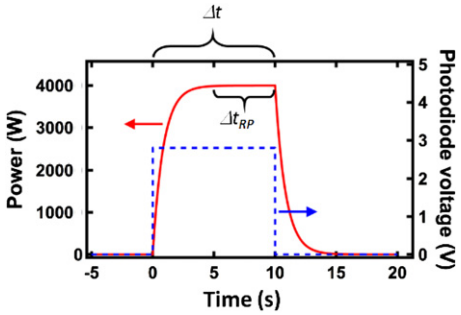

Figure 2. Illustration of symbiotic relationship between laser power measured by radiation pressure (solid (red) line, left axis) and that using the photodiode (dashed (blue) line, right axis). Δt is the total injection period of the laser and Δt_{RP} is the period of the injection for which laser power is measured with radiation pressure.

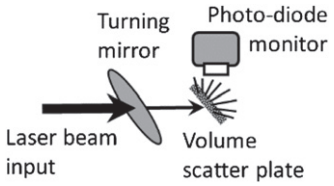

Figure 3. Detail of photodiode-based laser sampling setup. The full laser beam is incident on the first turning mirror with a transmission of (10–20) ppm. This severely attenuated beam is incident on a volume scattering plate at a 45° angle. Scattered light exits with a wide divergence angle and significantly reduced coherence. An unspecified fraction of this light is incident on the photodiode.

photodiode response (including the coupling ratio between total laser power and that captured by the photodiode) by comparison with the simultaneously acquired radiation pressure power measurement.

This concept has been discussed previously [3] but not fully implemented. It is accomplished here as follows. For a laser injection, a measurement of laser power using both the radiation pressure approach and the photodiode voltage will produce results as shown schematically in figure 2. The radiation-pressure-based power measurement is a high-accuracy result but with a slow response time. Alternatively, the photodiode risetime is much faster, showing no noticeable response time (at our current 10 Hz sampling rate) but has a prohibitively large uncertainty. By averaging the radiation-pressure-derived laser power over a suitable time period, we can compare to the average voltage from the photodiode during that same time interval and thus calibrate the photodiode response. This produces a calibration factor C_{PD} for the photodiode

$$C_{\mathrm{PD}} = \frac{\langle V_{\mathrm{PD}} \rangle_{\Delta t_{\mathrm{RP}}}}{\langle P_{\mathrm{RP}} \rangle_{\Delta t_{\mathrm{RP}}}}, \tag{5}$$

where V_{PD} is the photodiode voltage, P_{RP} is the laser power measured by radiation pressure, and the angled brackets $\langle \blacksquare \rangle_{\Delta t_{\mathrm{RP}}}$ indicates an average of the argument over the period Δt_{RP}. This has the significant effect of providing an *in situ* calibration of the photodiode valid for the exact conditions of the laser injection. This *in situ* calibration permits traceable measurements of total laser power with a response time that is independent of the force sensor and only limited by the response time of the photodiode. This concept could be applied to modulated or pulsed laser power. The requirement is that the average laser power during the calibration interval be sufficiently strong to be measurable by the radiation pressure portion of the AFR and that the photodiode response is sufficiently linear over the range of the measurement.

This approach can also mitigate drift typically seen by force balances over long measurement durations. Typically, thermal drift of force responsivity must be corrected in analytical balances by comparing the unloaded (background or 'tare') mass reading to the loaded reading. We currently perform a similar correction by reading the force on the sensor before, during, and after the laser injection. The pre- and post-injection force measurements are used to correct for any linear (with time) drift in the responsivity of the force balance during the injection. This is detailed in [2]. However, this correction assumes a linear drift of the force responsivity with time. We have found empirically that for injections longer than about 60 s (depending on environmental conditions and laser-induced heating) the force balance can drift in a fashion that is not linear with time. This currently limits radiation pressure measurements for long injection times. However, since the photodiode signal is not susceptible to this drift, we could use it as a reference to distinguish drift of the force sensor from drift of the laser power permitting a traceable measure of laser power regardless of the injection duration. This approach makes the assumption that the transmission of the turning mirror is stable during the injection and that the pre- and post-injection taring operations avoid data sampled during the rise or fall time of the force sensor as in [2].

While the photodiode need not fully sample the beam, this approach does require that the fraction of the beam which is sampled by the photodiode be stable throughout the duration of the laser injection. Instability could come from wander in the position of the beam, modal instability of the laser or delivery fiber, speckle effects, and polarization instability. We mitigate these effects using the setup shown in figure 3. The (10–20) ppm fraction of the laser beam that is transmitted through the first turning mirror is incident on a volume scattering plate oriented at 45° to the incoming beam. The small fraction of the light that emerges from the scattering plate is sufficiently incoherent and uniform to permit a much more stable power measurement on the photodiode. As mentioned, the true fraction of light reaching the photodiode need not be known since it is contained within the calibration of equation (5).

To quantify the extra noise incurred due to the photodiode, we measured the fractional standard deviation of the photodiode voltage during injection with a Gaussian beam to be 0.002. To test the worst-case variation in photodiode voltage due to spatial instability of an incoming beam, we used a laser with an asymmetric, non-Gaussian beam with spatial 'hot-spots' of higher powers and wiggled the laser's multimode delivery fiber during the injection. We found the fractional standard deviation of the photodiode signal increased to 0.015 under these conditions with the increase attributable to spatial instability of the laser beam.

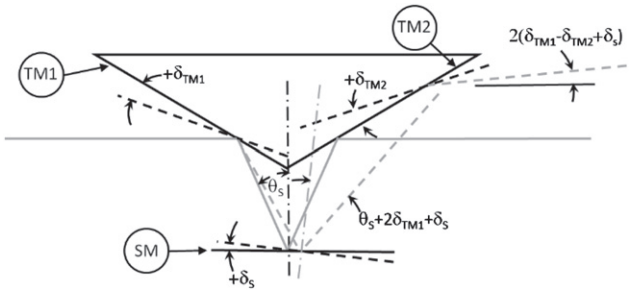

Figure 4. Diagram of AFR power meter showing the effect of misalignments on the angle of incidence on the sensing mirror. Solid black lines give the ideal position of the components; dashed black lines are represent their potential misalignment. Grey solid lines are the ideal laser beam path; grey dashed lines are the beam path for misalignments. TM1 is the entrance turning mirror, TM2 is the exit turning mirror, and SM is the sensing mirror. θ_S is the ideal incidence angle on the sensing mirror; δ_{TM1}, δ_{TM2}, and δ_S are the misalignment angles of the three mirrors.

3. Measurement uncertainty

3.1. Mirror

There are two sources of error related to the sensing mirror. The first is accuracy in the knowledge of the mirror's optical parameters (reflectance, scattering, absorptance, and transmission) at the laser wavelength in question. The second is accurate knowledge of the laser beam's angle of incidence θ onto the sensing mirror.

Since the error in the angle of incidence between the laser beam and the sensing mirror cannot be directly measured due to the enclosed design of the assembled AFR, it must be estimated from the laser beam's alignment with the plane of the entrance aperture and the geometrical tolerances of the assembled instrument.

The AFR is designed so that a horizontally travelling laser beam will hit the entrance turning mirror at an incidence angle of $\theta_{TM} = 56°$ then reflect to make an incidence angle of $\theta_S = 22°$ on the sensing mirror and a symmetric angle θ_{TM} on the exit turning mirror. However, as shown by figure 4, angular misalignment of the entrance turning-mirror or the sensing mirror will cause an error in the angle of incidence with the sensing mirror. In addition, if the incoming laser beam is not horizontal, it will add to the error. If the entering laser beam is tilted downward by an angle δ_{in}, the true angle of incidence θ on the sensing mirror will be given as

$$\theta = \theta_S + \delta_\theta = \theta_S + \delta_{in} + \delta_S + 2\delta_{TM1} \tag{6}$$

where δ_θ represents the sum of the alignment errors δ_{in}, δ_S, and δ_{TM1} are described above and in figure 4.

We assess the uncertainty values associated with equation (6). The angular alignment of the turning mirrors comes from two steel pin supports mounted into both side panels of the AFR housing. The position tolerance of the placement of these pins yields a standard uncertainty for turning mirror alignment angle of 0.64 mrad. We measured the worst-case deviation angle of the sensing mirror away from horizontal and assign it a standard uncertainty of 2.4 mrad. The infrared input laser beam (wavelength 1070 nm) is aligned to the horizontal using the visible (red) guide beam which permitted an alignment standard uncertainty of 5 mrad. Adding these in quadrature yields the angular error δ_θ as having a zero mean and a standard uncertainty of $\sigma_\theta = 5.6$ mrad.

The angle of incidence θ on the sensing mirror in equations (1) and (5) is a compound angle such that

$$\cos(\theta) = \sqrt{1 - \sin^2(\theta_S + \delta_\theta) - \sin^2(\theta_R)} \tag{7}$$

with θ_R representing tilt of the beam on the sensing mirror perpendicular to the direction of θ_S. This angle is related to the angle of rotation θ_Z of the AFR about its vertical axis as $\tan(\theta_R) = \frac{\tan(\theta_Z)}{\cos(\theta_S)}$ with $\theta_Z = \theta_R = 0$ for perfect alignment. From equations (1), (6) and (7) the relative standard uncertainty contribution of angular error to measured laser power is given (to first order) as

$$u_\theta \approx \tan(\theta_S)\,\sigma_\theta, \tag{8}$$

which for our target sensing mirror angle of $\theta_S = 22°$ is $u_\theta = 0.0023$. This illustrates an advantage of the AFR design from the standpoint of operator alignment. To first order, the reported power is unaffected by small rotational misalignment in θ_Z. Angular deviation of the incoming beam from horizontal does have an effect but the $\theta_S = 22°$ angle of incidence with the sensing mirror reduces by 60% the resulting power error compared with an instrument with an angle of incidence target of 45°.

Uncertainty in mirror reflectivity directly contributes to the uncertainty of power measurement. With reflectivity values typically between 0.999 98 and 0.999 99, we measure mirror reflectivity as the fraction of non-transmitted light. This technique has been described previously [2] and accounting for possible light scattering and absorption in the fused silica substrates yields a standard uncertainty of 0.000 43 per mirror. In the case of the AFR, the measured result involves light reflected from two mirrors (the first turning mirror and the sensing mirror) adding the uncertainty in quadrature gives a total standard uncertainty $u_r = 0.0006$ for the mirrors.

The alignment imperfections described above not only contribute to uncertainty in laser power measurement, but they also produce an angular error between the output and input beams. As mentioned, we desire coaxial input and output beams to simplify measurement setup. We measure the angular misalignment by using the visible alignment laser. We can remove the photodiode assembly from the AFR so that one input beam produces two outputs—the regular beam which is reflected from the three mirrors and a weaker beam which is transmitted through both of the turning mirrors. The mirrors are coated for high reflectivity at the 1070 nm operating wavelength and but only moderate reflectivity (∼50%) for the red alignment beam. This allows us to view both the unperturbed (input) and reflected (output) beams simultaneously. We measured a 5 mrad angle between the two beams. We can force these two beams to co-align by either tilting the incoming laser beam or the AFR. This technique may reduce or increase the angular error on the sensing mirror and thus the power measurement error depending on the source of the

Table 1. Noise on force sensor due to air currents and vibrational noise. NEP is the noise-equivalent power.

Number of windows installed	Noise standard deviation σ_n (W)	NEP (W Hz$^{-1/2}$)
0	73.7	46.6
1	3.26	2.06
2	3.70	2.34

original misalignment. We follow this procedure to force well-aligned input and output beams. Evaluating the potential alignment errors of figure 4, we find the standard relative uncertainty incurred by forcing the two output beams to align is $u_a = 0.001$.

3.2. Force sensor

The force on the sensing mirror is measured with a commercial force balance. Uncertainty in the response of such a device comes from three sources—sensor calibration, air currents and acoustic vibration, and inherent force balance repeatability and drift nonlinearity. Since the power measurement comes from the difference of measured force with and without the laser beam, the orientation of the force sensor with respect to gravity has no effect on the measured power and therefore does not contribute to measurement uncertainty.

3.2.1. Sensor calibration. From equation (1), a laser power of 1 kW incident on a perfect mirror at an incidence angle of 22° will produce a force of 6.186 μN which is the weight of a 631 μg mass. To assess the uncertainty of the force balance contribution at such small mass values, we have calibrated our balance using a set of wire calibration masses ranging in value from 162 μg to 48 mg. These wires were assigned SI traceable mass values using the NIST electrostatic force balance [17]. They were in turn used to calibrate the AFR's force balance over the same range. This process is described in detail in [18] and yields a relative standard uncertainty of $u_F = 0.0025$ due to the force balance calibration.

3.2.2. Acoustic noise and air currents. As with any sensitive force balance, acoustic vibrations and air current incident on the sensing mirror are noise sources. Fortunately, response time of this type of force balance (on the order of 5 s) filters out much of the acoustic noise which tends to be of higher frequencies. Air currents can be significantly reduced by covering the entrance and exit ports of the AFR with anti-reflection-coated windows. However, even with the 0.1% reflection (per surface) afforded by the coatings, power reflected from the window surfaces can present safety issues when incident powers are of tens of kilowatts. As such, operation without windows is preferred. To assess the mitigation of air current effects, we measured the raw output of the force balance as a function of time with two, one, and no windows in place. This commercial balance reports its measurements in units of mass but we convert this to a force using the acceleration of gravity g and then to a power using equation (1). With no laser injection, we sampled this power for tens of seconds and measured the standard deviation. Table 1 reports the measured noise in terms of standard deviation σ_n and noise equivalent power (NEP), which is found as

$$\mathrm{NEP} = \sigma_n \sqrt{\tau} \tag{9}$$

where $\tau = 0.4$ s is the measured rise time (1/e point of the exponential rise) of the force balance.

We find that the installation of just one window drastically improves the noise level over that of no windows while the addition of the second window has no significant effect on the noise. As an example of this noise contribution, the single-window NEP predicts a measurement standard deviation of $u_{NEP} = 0.92$ W for a 5 s measurement duration.

3.2.3. Balance repeatability and nonlinear drift. In a slightly different experiment, we used the AFR (with one aperture open) to measure the average laser power during multiple laser injections lasting 30 s each. We performed 5–10 injections at each of five laser power levels—nominally 1 kW, 2.5 kW, 5 kW, 7.5 kW, and 11 kW. Each injection yielded an average power (over the 30 s injection duration). We calculated the standard deviation σ_P these measured averages for each of the power levels. We found σ_P to be largely independent of the injected laser power level with an average value of $\sigma_P = 9.97$ W. This result is significant in that it is not predicted by the air current noise of table 1. Specifically, for a 30 s average, the NEP for one installed window would predict a 30 s standard deviation of 0.38 W. We assign this 9.97 W noise to force balance repeatability and define the standard uncertainty due to total random noise sources u_N (for a 30 s injection, under conditions similar to our laboratory) as the quadrature sum of σ_P and σ_n so that $u_N = 10$ W.

A similar effect is due to laser-induced thermal drift of the force balance response. Depending on the layout of the power measurement, the high-power laser beam can heat the force balance—through absorption by the window or scattered light or heat from a nearby beam dump. Typically, force balances are temperature compensated, but there will always be some residual dependence on temperature or its gradient. This effect is identified as a measured force that changes with time when a constant-power laser beam is incident on the sensing mirror. The baseline correction algorithm removes any drift slope that is constant with time. But any non-linear residual ('drift nonlinearity') remains. This shows up as a power dependence to the standard deviation in measured power. The repeatability of measured power had the power-independent component σ_P described above as well as a power-dependent portion $\gamma_T = 0.0006$. This value is about one half of what was measured for the RPPM implementation [2]. We attribute this reduced environmental dependence to the AFR design that has

Table 2. Uncertainty components for axial force radiometer (AFR). Type A represents uncertainties which are statistically determined, and type B are those determined through other means. All are represented as relative standard uncertainties.

	Type A	Type B
Sensing mirror angle, u_θ		0.0023
Mirror reflectivity, u_r		0.0006
Force sensor calibration, u_F		0.0025
Forced alignment, u_a		0.001
Balance repeatability, u_N	10 W	
Drift nonlinearity, γ_T	0.0006	

the force balance enclosed within the housing exposing it to less external heating effects than the RPPM.

3.3. Combined uncertainty

We estimate the expanded fractional uncertainty U on the power measurement as the quadrature sum of the various components detailed above and summarized in table 2.

These uncertainty elements combine to give the relative expanded uncertainty on the AFR power measurement

$$U(P,\Delta t) = 2\sqrt{u_\theta{}^2 + u_\mathrm{r}{}^2 + u_\mathrm{F}{}^2 + u_\mathrm{a}{}^2 + \gamma_\mathrm{T}{}^2 + \left(\frac{u_\mathrm{N}}{P}\sqrt{\frac{30}{\Delta t}}\right)^2}, \tag{10}$$

where the coverage factor of $k = 2$ [19] defines an interval having a level of confidence of approximately 95% [20]. Upon inserting values from table 2 for a nominal injection time of 30 s, we find that for power levels between 1 kW and 2 kW, the nominal expanded uncertainty is 2.1% and above 2 kW, the expanded uncertainty is 1.2%.

4. Validating measurements

As a primary standard, the AFR derives its uncertainty and traceability through the kilogram. However, as a validation of our uncertainty analysis, we have performed a power comparison between the RPPM (also a primary standard) and the AFR. The experimental setup is shown in figure 5.

The non-exclusive nature of radiation pressure as a means to measure laser power enables the unique power meter comparison setup of figure 5. That is, we can measure the total power in a laser beam using two different power meters simultaneously. We used a Yb-doped fiber laser at a wavelength of 1070 nm to produce a collimated beam that first passes through the AFR and then the RPPM. The laser collimator was positioned adjacent to the entrance aperture with a non-contacting air-baffle collet to limit air flow through the entrance aperture which eliminated the need for an input window (favorable for safety). The collimator did not make physical contact with the AFR body or the air-baffle collet in order to minimize vibrational coupling from the flow of cooling water through the collimator head or of motions of the process fiber connecting the collimator to the laser. The output aperture was left open.

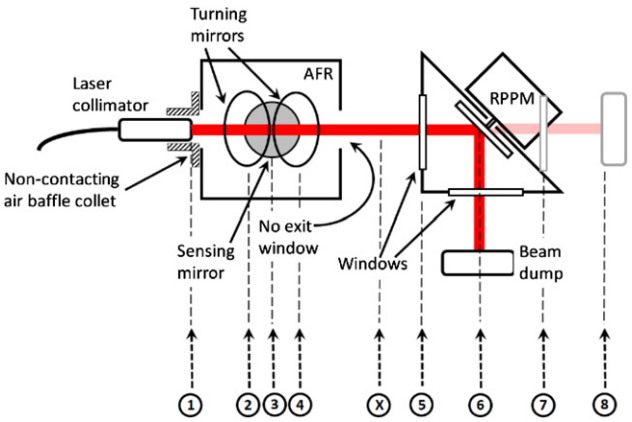

Figure 5. Plan view of the experimental setup for comparison between AFR and RPPM. Labeled positions 1–8 indicate reflecting surfaces (weak or strong) that will affect the forward and reverse propagating power in the laser beam. Position '*X*' is the point between the 2 m at which the measured power is referenced. Gray elements represent schematic positions of the RPPM exit window and beam dump for the sake of marking the position of surfaces 7 and 8.

This unique simultaneous power measurement greatly simplifies the process of comparing power meters, but also introduces new considerations. To relate the power measured simultaneously by each of these radiation pressure devices, we must be clear on the longitudinal position at which the power is being measured. In other words, each power meter measures the power that impinges on its sensing mirror. However, because of finite transmission, absorption, and scattering from the sensing mirror, the optical power impinging on the sensing mirror is minutely greater than the optical power that is reflected from the mirror. The high reflectivity of our mirrors makes this difference insignificant in practice. However, effects of non-zero window reflectances are not negligible. When windows are in place between the power meters, we must consider not only the effect of their optical loss (due to reflection) on the downstream power meter, but also the effect of light reflected from the intermediate window back onto the sensing mirror of the upstream power meter. Thus an intermediate window will cause an increase in the measured power by the upstream power meter and a decrease in the measured power by the downstream power meter. These back reflection and loss mechanisms have an effect equal to roughly twice the reflectivity of the window. The broad spectral shape of the laser light [on the order of (5–10) nm] ensures that we need not consider interference effects from the multiple surfaces of these reflective elements labelled in figure 5 with numbers 1–8.

Figure 5 illustrates the various reflecting surfaces that must be considered in this comparison. Practically, reflective surfaces upstream of the first power meter or downstream of the second power meter have no net effect for the sake of comparison since their presence has the same effect on both power meters. This equivalence assumes the windows are aligned such that the laser beam is incident normally.

We chose to perform the comparison by converting the power reported at each power meter to the power that is

expected at the point labeled 'X' in figure 5. We do this using window reflectivity values measured analogous to what was done for the mirrors [2]. With reflectivities of 0.999 98 to 0.999 99, our mirrors (surfaces '3' and '6' in figure 5) contribute negligible loss to the power budget. With no output window on the AFR, there is only one window (two reflective surfaces) between AFR and RPPM sensing mirrors—it is the RPPM's upstream shielding window (surface '5' in figure 5). The absorption loss coefficient for fused silica is on the order of 1.7×10^{-4} mm^{-1} [21] which produces a negligible loss in the 1 mm thick substrate. The window has an anti-reflection coating with a reflectivity of $R_w = 0.0001$ per surface.

To accurately compare the simultaneous measurement results of two radiation-pressure-based laser power meters, we must select a position y along the beam path at which the powers will be compared. We denote the forward-propagating power at this point as P_y. A given power meter will report the total power incident on its sensing mirror as P_{mirror}. This value includes both the forward-propagating power at the sensing mirror as well as any back-reflected power from reflecting surfaces downstream of the mirror. The relationship between P_{mirror} and P_y depend on the number K of reflecting surfaces downstream of the sensing mirror, and the number M of reflecting surfaces between the sensing mirror and position y. The relationship is then

$$P_y = \frac{P_{\text{mirror}}(1-R_w)^{\gamma M}}{\left(1+R_w\sum_{i=1}^{K}(1-R_w)^{i-1}\right)}, \tag{11}$$

where it is assumed that all reflecting surfaces have the same reflectivity R_w, $\gamma = +1$ when the sensing mirror is upstream of point y and $\gamma = -1$ when the sensing mirror is downstream of y. The reflectivity term in the numerator compensates for losses between the mirror and point y due to reflections and the reflectivity term in the denominator compensates for the extra force on the mirror due to reflected light. For anti-reflection coated surfaces, $R_w \ll 1$, and we can ignore terms of order higher than R_w. This yields

$$P_y \approx \frac{P_{\text{mirror}}\,(1-\gamma M R_w)}{(1+KR_w)}. \tag{12}$$

In the case of our comparison measurement (figure 5) we apply equation (12) to the power measured by the AFR and the RPPM to produce the power each predicts for the common position X (figure 5) as $P_{\text{AFR},X}$ and $P_{\text{RPPM},X}$ respectively. With the low reflectivity of our windows ($R_w = 0.0001$) the fractional correction is small with a magnitude of 0.0004 and whose uncertainty contribution to the overall power measurements is negligible. The fractional error in the comparison measurement is then

$$\frac{\Delta P}{\langle P\rangle} = 2\frac{P_{\text{AFR},X} - P_{\text{RPPM},X}}{P_{\text{AFR},X} + P_{\text{RPPM},X}}. \tag{13}$$

To assess the validity of the AFR measurements, we compare the magnitude of this fractional error to the quadrature sum of the uncertainties of the two measurement techniques. This is plotted in figure 6. We find the average discrepancy (the quantity of equation (13) expressed as a percent) between the two techniques for powers ranging from 1 kW to 10.8 kW is 0.12% and within 0.5% for all cases. This is well within the combined expanded uncertainty of the two techniques.

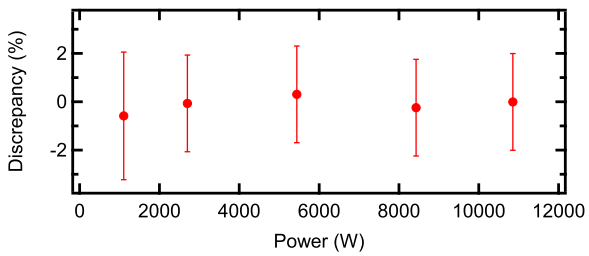

Figure 6. Discrepancy between AFR and RPPM power values. Discrepancy is the quantity of equation (13) expressed as a percent. The error bars represent the quadrature sum of the expanded uncertainties of the AFR and RPPM measurements.

5. Conclusions

The 0.12% agreement between AFR and RPPM validates our uncertainty analysis of the AFR for power levels from 1 kW to 10.8 kW. The uncertainty analysis of section 4 yields the expanded uncertainty specifically described by equation (10) and table 2. But for general conditions we describe the expanded uncertainty as 2.1% from 1 kW to 2 kW and 1.2% above 2 kW (for an approximate 95% confidence interval). While the fractional uncertainty tends to improve with increased signal (laser power), we expect that ultimately at the highest powers, thermal affects associated with laser heating will dominate the uncertainty.

A goal of the development of AFR is to yield a design that can be easily duplicated and used with a variety of commercial analytical balances. As such, we will provide mechanical drawings of the housing design on request.

Future development work with the AFR will focus on testing at higher powers, and further development of the photodiode implementation. We see a promise in this photodiode-radiation-pressure combination to significantly increase the measurement bandwidth—eventually enabling radiation-pressure based measurements of single-pulse energy measurements below the current 200 J threshold of the RPPM [22].

Acknowledgments

This work was partially funded by the U.S. Naval Surface Warfare Center.

ORCID iDs

Paul A Williams https://orcid.org/0000-0001-8419-7434
Kyle A Rogers https://orcid.org/0000-0003-2470-5286
Joshua A Hadler https://orcid.org/0000-0003-2730-578X
Alexandra B Artusio-Glimpse https://orcid.org/0000-0002-8289-2393
John H Lehman https://orcid.org/0000-0003-4729-7123

References

[1] Thoss A 2020 Leverage the Change https://laserfocusworld.com/blogs/article/14074862/2020-leverage-the-change

[2] Williams P *et al* 2017 Portable, high-accuracy, non-absorbing laser power measurement at kilowatt levels by means of radiation pressure *Opt. Express* **25** 4382–92

[3] Williams P A, Artusio-Glimpse A B, Hadler J A, King D W, Rogers K A, Ryger I, Vo T and Lehman J H 2019 Radiation-pressure enabled traceable laser sources at CW powers up to 50 kW *IEEE Trans. Instrum. Meas.* **68** 1833–9

[4] Lehman J H, Rogers K, Rahn D and Williams P 2019 Inline laser power measurement by photon momentum *Appl. Opt.* **58** 1239–41

[5] Nichols E E and Hull G F 1903 The pressure due to radiation *Phys. Rev.* **17** 25

[6] Lebedev P N 1901 Experimental examination of light pressure *Ann. Phys.,* **6** 1–26

[7] Stimler M, Slawsky Z I and Grantham R E 1964 Torsion pendulum photometer *Rev. Sci. Instrum.* **35** 311–3

[8] Cook J J, Flowers W L and Arnold C B 1962 Measurement of laser output by light pressure *Proc. IRE* **50** 1693

[9] Yuan Y 1990 A new pulse laser energy meter *Rev. Sci. Instrum.* **61** 1743–6

[10] Agatsuma K, Friedrich D, Ballmer S, DeSalvo G, Sakata S, Nishida E and Kawamura S 2014 Precise measurement of laser power using an optomechanical system *Opt. Express* **22** 2014–31

[11] Nesterov V, Mueller M, Frumin L L and Brand U 2009 A new facility to realize a nanonewton force standard based on electrostatic methods *Metrologia* **46** 277–82

[12] Wilkinson P R, Shaw G A and Pratt J R 2013 Determination of a cantilever's mechanical impedance using photon momentum *Appl. Phys. Lett.* **102** 184103

[13] Ma D, Garrett J L and Munday J N 2015 Quantitative measurement of radiation pressure on a microcantilever in ambient environment *Appl. Phys. Lett.* **106** 091107

[14] Shaw G, Stirling J, Kramar J, Williams P, Spidell M and Mirin R 2018 Comparison of electrostatic and photon pressure force references at the nanonewton level *Metrologia* **56** 025002

[15] Artusio-Glimpse A B, Ryger I, Azarova N A, Williams P A, Hadler J A and Lehman J H 2020 Miniature force sensor for absolute laser power measurements via radiation pressure at hundreds of watts *Opt. Express* **28** 13310–22

[16] Stoney G G 1909 The tension of metallic films deposited by electrolysis *Proc. R. Soc.* A **82** 172–5

[17] Shaw G A and Stirling J 2019 Measurement of submilligram masses using electrostatic force *IEEE Trans. Instrum. Meas.* **68** 2015–20

[18] Rogers K A, Williams P A, Shaw G A and Lehman J H 2020 Simplified kilogram traceability for radiation pressure based laser power meters *Appl. Opt.* **59** 8719–23

[19] Joint Committee for Guides in Metrology 2008 JCGM 100:2008, evaluation of measurement data—guide to the expression of uncertainty in measurement (GUM 1995 with minor corrections) (Paris, France: Joint Committee for Guides in Metrology)

[20] Taylor B N and Kuyatt C E 1994 Guidelines for evaluating and expressing the uncertainty of NIST measurement results *NIST Tech. Notes* 1297

[21] Yang S T, Matthews M J, Elhadj S, Cooke D, Guss G M, Draggoo V G and Wegner P J 2010 Comparing the use of mid-infrared versus far-infrared lasers for mitigating damage growth on fused silica *Appl. Opt.* **49** 2606–16

[22] Williams P, Rogers K, Hadler J, Lee R and Lehman J 2019 Using photon momentum to measure high CW laser power and pulse energy *Proc. SPIE* **11033** 110330A